

Published in final edited form as:

Nature. 2020 March ; 579(7798): 240–244. doi:10.1038/s41586-020-2069-3.

Ru isotope vestige of Earth's pre-late veneer mantle preserved in Archean rocks

Mario Fischer-Gödde¹, Bo-Magnus Elfers¹, Carsten Münker¹, Kristoffer Szilas², Wolfgang D. Maier³, Nils Messling¹, Tomoaki Morishita^{4,5,6}, Martin Van Kranendonk⁷, Hugh Smithies⁸

¹Institut für Geologie und Mineralogie, University of Cologne, Zùlpicher Str. 49b, 50674 Köln, Germany

²Department of Geosciences and Natural Resource Management, University of Copenhagen, Øster Voldgade 10, 1350 Copenhagen, Denmark

³School of Earth and Ocean Sciences, Cardiff University, Park Place, Cardiff, UK

⁴Faculty of Geosciences and Civil Engineering, Institute of Science and Engineering, Kanazawa University, Kanazawa, Ishikawa 920-1192, Japan

⁵Lamont-Doherty Earth Observatory, Columbia University, New York, NY 10027, USA

⁶Volcanoes and Earth's Interior Research Center, Japan Agency for Marine-Earth Science and Technology, 2-15 Natsushima, Kanagawa, 237-0061, Japan

⁷Australian Centre for Astrobiology, University of New South Wales, Sydney, Australia

⁸Geological Survey of Western Australia, East Perth, WA, Australia

Abstract

The accretion of volatile-rich material from the outer solar system represents a crucial prerequisite for Earth developing oceans and becoming a habitable planet^{1–4}. However, the timing of this accretion remains controversial^{5–8}. It was proposed that volatile elements were added to Earth by late accretion of a late veneer consisting of carbonaceous chondrite-like material after core formation had ceased^{6,9,10}. This view, however, could not be reconciled with the distinct ruthenium (Ru) isotope composition of carbonaceous chondrites^{5,11} compared to the modern mantle¹², and in fact also not with any known meteorite group⁵. As a possible solution, Earth's pre-late veneer mantle could already have contained a significant amount of Ru that was not fully extracted by core formation¹³. The presence of such pre-late veneer Ru could only be proven if its

Users may view, print, copy, and download text and data-mine the content in such documents, for the purposes of academic research, subject always to the full Conditions of use:http://www.nature.com/authors/editorial_policies/license.html#terms

Correspondence and requests for materials should be addressed to M.F.-G. (mfisch48@uni-koeln.de).

Author contributions

M.F.-G. and C.M. designed the project. M.F.-G., B.-M. E. and N.M. developed the analytical method and obtained the Ru isotope data. M.F.-G. wrote the manuscript. All authors contributed to the discussion of the results and editing of the manuscript.

Competing interests

The authors declare no competing interests.

Data availability

The data that support the findings of this study are available from the EarthChem library (URL: <https://doi.org/10.1594/IEDA/111462>).

isotope composition would be distinct from that of the modern mantle. Here we report the first high-precision mass-independent Ru isotope compositions for Eoarchean ultramafic rocks from SW Greenland, which display a relative ^{100}Ru excess of +22 parts per million compared to the modern mantle value. This ^{100}Ru excess indicates that the source of the Eoarchean rocks already contained a significant fraction of Ru prior to the late veneer. By 3.7 Gyr the mantle beneath the SW Greenland rocks had not yet fully equilibrated with late accreted material. Otherwise, no Ru isotopic difference relative to the modern mantle would be observed. By considering constraints from other highly siderophile elements beyond Ru¹⁴, the composition of the modern mantle can only be reconciled if the late veneer contained significant portions of carbonaceous chondrite-like materials with their characteristic ^{100}Ru deficits. These data therefore relax previous constraints on the late veneer and now permit that volatile-rich material from the outer solar system was delivered to Earth during late accretion.

Ruthenium is a highly siderophile element (HSE) and is therefore expected to be sequestered into the metallic core during Earth's differentiation. Contrary to this prediction, the abundances of Ru and other HSEs in the modern mantle are higher than expected compared to metal-silicate equilibrium conditions^{15,16}. This observation is most commonly explained by HSE replenishment of the mantle through addition of a 'late veneer' after core formation. Approximately chondritic relative abundances of HSEs in the mantle suggest that the late veneer must have consisted of primitive meteoritic material^{17,18}, amounting to ~0.5% of the Earth's mass¹⁸. The chemical composition of the late veneer and its origin are a longstanding matter of debate, especially in the context of how and when Earth accreted its water and volatiles^{3,6,9,10}. In this regard, previous studies debated whether significant amounts of volatile-rich carbonaceous chondrite-like material were added by the late veneer during the final stages of Earth's accretion^{6,9,10} or had already been incorporated during earlier stages of Earth's growth^{3,5,7,8,11}.

Mass-independent ruthenium isotopic variations among meteorites and the Earth have provided evidence that the late veneer was derived from reduced and volatile-poor inner solar system materials most similar to enstatite chondrites^{5,11,12,19}. This is in contrast to constraints from relative abundances of volatile elements such as selenium (Se) – tellurium (Te) – sulphur (S) and the Se isotope composition in the silicate Earth that were used to argue for a CM or CI carbonaceous chondrite-like late veneer composition^{2,9,10}. Owing to its distinct Ru isotope composition, volatile-rich carbonaceous chondrite-like material from the outer solar system was excluded as possible late veneer source material^{5,11} and thus, the late veneer appeared unlikely to be the primary source of water and volatiles on Earth^{5,11}. It should be noted, however, that this conclusion depends on the premise that the Ru in the Earth's mantle originates solely from the late accreted materials that were added after cessation of core formation^{11,15,16,18}. If, however, the Earth's pre-late veneer mantle retained a significant fraction of Ru during metal-silicate differentiation^{13,20}, as recently suggested, this conclusion would be invalid. Thus, investigating Ru isotope signatures in the putative remnants of pre-late veneer mantle would not only reveal new insights into the timescales and efficiencies of mixing the late veneer into the Earth's mantle, but also new constraints on the composition of the material that was added as a late veneer.

Until now, however, no unambiguous isotopic evidence for the preservation of pre-late veneer mantle on Earth exists. For instance, resolvable excesses in ^{182}W reported for 3.8 Gyr-old Archean rocks from Isua (Greenland) and Acasta (Canada) in conjunction with relatively low HSE abundances observed in 3.5–3.2 Gyr-old Archean komatiites from the Pilbara craton (Australia) and the Barberton greenstone belt (South Africa) were interpreted to reflect sluggish mixing of the late veneer into the early Archean mantle^{21,22}. However, it was later suggested that the mantle sources of the 3.8–3.7 Gyr-old Isua supracrustal belt (ISB) rocks, including 3.8 Gyr-old Eoarchean peridotites from Narssaq ultramafic body (NUB) and the south of the Isua supracrustal belt (SOISB), already had HSE abundances at about ~60–100% of the modern mantle value^{14,23}. This suggests that by ~3.8 Gyr the late veneer was to a large extent mixed into the ambient mantle. To reconcile ^{182}W excesses with the presence of modern mantle-like HSE abundances it was proposed that a small amount of core material could have been entrained into the proto-Earth's mantle as a consequence of the Moon-forming giant impact^{20,24}. Furthermore, ^{182}W anomalies could also be generated by early mantle differentiation processes during the first ~50 Myrs of the solar system^{25–29} or by core mantle interaction in the source of mantle plumes³⁰. In summary, ^{182}W and HSE concentration data alone fail to provide an unambiguous test as to whether pre-late veneer mantle domains were indeed preserved.

Here we explore the potential of mass-independent Ru isotope variations in terrestrial rocks as a new tool to investigate whether pre-late veneer isotope signatures can be found in the Archean mantle. While the Ru isotope composition of the modern mantle is well-constrained¹², this is not the case for the Archean mantle. To address this issue, we determined the Ru isotope composition for a set of ultramafic rocks from different Eoarchean and Paleoproterozoic terranes (Extended data Table 1, see Methods for details). Herein, we focus on the $^{100}\text{Ru}/^{101}\text{Ru}$ and $^{102}\text{Ru}/^{101}\text{Ru}$ ratios to constrain the Ru isotope compositions of the mantle sources of these rocks because these are the isotope ratios measured at the highest precision and they also show the largest variability among meteoritic materials^{5,19,31}. The results are reported as ϵ -unit (0.01%) deviations of mass bias-corrected $^{100}\text{Ru}/^{101}\text{Ru}$ and $^{102}\text{Ru}/^{101}\text{Ru}$ from a terrestrial standard.

Exotic composition of Archean mantle

We report Ru isotope data for samples from four different cratons. The Ru isotope compositions obtained for ultramafic samples from the Pilbara craton, the Superior Province (Abitibi greenstone belt) and the Kaapvaal craton (Bushveld Complex) are indistinguishable from the Ru solution standard (Fig. 1), indicating that their Ru isotope composition reflects that of the modern terrestrial mantle. By contrast, Eoarchean 3.8–3.7 Gyr-old ultramafic rocks from the North Atlantic craton, originating from various localities of the Itsaq gneiss complex (IGC) in SW Greenland (NUB, SOISB, ISB, and the Ujaragssuit Nunât layered intrusion) exhibit a uniform and well-resolved excess in $\epsilon^{100}\text{Ru}$ of $+0.22 \pm 0.04$ (95% confidence interval, Fig. 1) combined with a smaller excess in $\epsilon^{102}\text{Ru}$ of $+0.09 \pm 0.02$ (95% confidence interval, Figure 2a). Chromitites from the younger 3.0 Gyr-old Seqi ultramafic complex in SW Greenland show the same excesses in $\epsilon^{100}\text{Ru}$ and $\epsilon^{102}\text{Ru}$. The combined $\epsilon^{100}\text{Ru}$ and $\epsilon^{102}\text{Ru}$ excesses in these rocks represent mass-independent isotope anomalies of nucleosynthetic origin and indicate that compared to the modern mantle the Ru in the SW

Greenland mantle source is enriched in nuclides produced by the slow neutron capture process (s-process) of nucleosynthesis (Fig. 2a). The isotope excesses cannot be explained by mass-independent fractionation effects or by inherited fissiogenic Ru nuclides (see Methods and Extended Data items for details about the accuracy of the Ru isotope data).

The s-process enriched composition inferred for the Archean SW Greenland mantle is an unexpected finding because compared to the Earth's modern mantle the Ru isotope compositions reported for all meteorites are deficient in s-process Ru and exhibit negative $\epsilon^{100}\text{Ru}$ and $\epsilon^{102}\text{Ru}$ anomalies^{5,19,31}. Therefore, the SW Greenland data for the first time provide unambiguous evidence for s-process enriched building material that contributed to the early stages of Earth's growth. Owing to the observed heliocentric zoning of $\epsilon^{100}\text{Ru}$ anomalies among meteorites⁵, we speculate that this reservoir was most likely located in the innermost region of the solar system, within < 1 AU (Fig. 2b).

Pre-late veneer Ru isotopic signature

The ^{100}Ru excess provides the first unambiguous evidence that the mantle source of the Greenland rocks did not receive the full complement of late veneer material²¹. Furthermore, it also requires that Ru and possibly other HSEs were not completely stripped from the mantle during the latest stages of core formation¹³. Otherwise, no Ru isotope anomaly could ever be observed. The uniform and ubiquitous presence of the $\epsilon^{100}\text{Ru}$ anomaly in various 3.8–3.7 Gyr-old ultramafic rock types from different Eoarchean terranes in Greenland (Isuakasia, Færingehaven) suggests that a larger mantle domain is lacking a full late veneer component^{20,21}. The presence of the $\epsilon^{100}\text{Ru}$ anomaly in the younger >3.0 Gyr-old chromitites from Seqi (Akia terrane) also indicates that even 700 Myrs later, the SW Greenland mantle had not fully equilibrated with the late veneer. Such a prolonged timescale for mixing-in of the late veneer component is consistent with significant HSE depletions observed in Archean mafic rocks from the Pilbara and Kaapvaal cratons²², which previously had been explained by sluggish inmixing of late veneer material.

As outlined above, the $\epsilon^{100}\text{Ru}$ excess identified in Eoarchean ultramafic rocks from SW Greenland indicates that Ru was not completely sequestered into the core, most likely because some late accretionary component was already delivered during the waning stages of core formation^{14,23,32}. Depending on the composition of this early late-veener material, the ^{100}Ru excess measured in the Greenland rocks would then represent a minimum estimate for the $\epsilon^{100}\text{Ru}$ excess of the pure pre-late veneer mantle. The nature of the early component that supplied the ^{100}Ru excess and was already mixed into the Greenland mantle before 3.8 Gyr, likely inner solar system material (Fig. 2b), can be further constrained by osmium (Os) isotope systematics. This is because the initial osmium isotopic compositions of chromitite and peridotite samples from the IGC overlap the $^{187}\text{Os}/^{188}\text{Os}$ composition of chondrites at 3.8 Gyr^{14,23,32,33} (Extended Data Table 2). Assuming that the positive $\epsilon^{100}\text{Ru}$ anomaly and the chondritic Os signature were both imparted by this component, it is unlikely that it is represented by any of the presently known chondritic meteorites because these all exhibit negative $\epsilon^{100}\text{Ru}$ values at chondritic Os isotope composition. Importantly, owing to its positive $\epsilon^{100}\text{Ru}$ value, this material cannot derive from a carbonaceous chondrite-like Moon-

forming impactor⁸ because carbonaceous chondrites also exhibit the most negative $\epsilon^{100}\text{Ru}$ values among all known chondrite groups⁵ (Fig. 2).

Carbonaceous chondrite-like late veneer

Regardless of the detailed nature and origin of the early accreted component, the ^{100}Ru excess inferred for the Eoarchean SW Greenland mantle source could only be balanced by addition of chondritic materials with negative $\epsilon^{100}\text{Ru}$ to yield the composition of the modern mantle ($\epsilon^{100}\text{Ru} = 0$). This mixing relationship is further illustrated in Figure 3, where possible $\epsilon^{100}\text{Ru}$ compositions for the pre-late veneer mantle are calculated by subtracting enstatite, ordinary or carbonaceous chondrite-like materials from the Ru isotopic composition of the modern mantle. The model is based on a recently proposed inefficient core formation scenario where about ~20% of the Ru (~1.4 ng g⁻¹) in the modern mantle derives from pre-late veneer stage¹³. Assuming a minimum late accretion contribution of 60% for the 3.8 Gyr Itsaq mantle source¹⁴, only the addition of a late veneer consisting of carbonaceous chondrites could account for $\epsilon^{100}\text{Ru} \approx 0$, as observed for the modern mantle¹² (Figure 3). The required proportion of late accreted material would amount to a maximum estimate of ~0.3% of the Earth's mass of average carbonaceous chondrite or CM carbonaceous chondrite material, consistent with a recent estimate based on Se isotopes¹⁰. A late veneer consisting of CM-like material is also supported by the abundance pattern of volatile elements in the silicate Earth^{2,9,10}. This conclusion remains robust, even if a larger fraction of Ru would have been present in the pre-late veneer mantle or if the late accretion component in the mantle by 3.8 Gyr was >60%, but in these cases a lower carbonaceous chondrite mass fraction would be sufficient. Ordinary chondrites would only become viable late veneer materials if the Greenland mantle by 3.8 Gyr contained a significantly lower late veneer contribution (<50%). Moreover, while a late veneer consisting of carbonaceous chondrites is in accord with the relative abundances of S-Se-Te and the Se isotopic composition of the modern mantle^{2,9,10}, the addition of a late veneer composed of ordinary chondrites cannot be reconciled with these constraints, because the relative abundances of S-Se-Te and the Se isotope composition of ordinary chondrites are markedly distinct from those of the Earth's mantle^{9,10}. If a major part of the late veneer would have consisted of core fragments from differentiated impactors²⁴, one potential caveat would be that this material cannot readily account for chondritic S-Se-Te and broadly chondritic HSE relative abundances in the Earth's mantle^{2,9,16,18}.

Collectively, our new data imply that the distinct ^{100}Ru isotope excess in the Eoarchean SW Greenland mantle source is best explained by late mixing of a carbonaceous chondrite-like late veneer fraction into the Earth's mantle. Thus, contrary to previous Ru isotope constraints on the late veneer^{5,18}, these data imply that significant amounts of volatile-rich outer solar system materials including water and volatiles were indeed added with the late veneer. This revised view is also in accord with other constraints such as those independently obtained from relative abundances and isotope compositions of Earth's volatile elements^{1,2,9,10}, which also indicate that the major share of Earth's volatiles was inherited from a carbonaceous chondrite source¹⁻⁴. Finally, our new data demonstrate that investigating the Ru isotope composition of terrestrial rocks represents a powerful and

distinctive tool to identify primordial mantle heterogeneities arising from incomplete equilibration of the ambient mantle with Earth's late stage building blocks.

Methods

Samples

The samples analyzed in this study comprise ultramafic rocks from four different cratons. The North Atlantic craton is represented by peridotite and chromitite samples of from various localities of the Eoarchean Itsaq gneiss complex (IGC) and the Mesoarchean Seqi ultramafic complex in southern W Greenland. The sample set is complemented by chromitites from the Kaapvaal craton (Bushveld Complex, South Africa) and the Pilbara craton (Australia), and a komatiite reference sample from the Superior Province (Abitibi greenstone belt, Canada). Where available, the Ru concentration and osmium isotope data of the samples analyzed in this study are given in Extended Data Table 2. For samples where no data were reported previously, Ru and Os data obtained for similar samples from the same location are listed.

The Itsaq gneiss complex (IGC) in SW Greenland represents one of the few worldwide localities where remnants of Eoarchean mantle are preserved. The IGC comprises two Eoarchean crustal terranes (Isuakasia and Færingehavn), where possible mantle rocks are exposed as ultramafic lenses in the 3.8-3.7 Gyr-old Isua supracrustal belt and ultramafic bodies in the 3.8 Gyr-old South of the Isua supracrustal belt (SOISB), both located in the Isuakasia terrane^{35,36}. In the Færingehavn terrane such rocks are exposed in the 3.8 Gyr-old Narssaq ultramafic body³⁷ (NUB). The peridotite and chromitite samples investigated in this study were selected to cover all of these different localities.

Samples 10-9 and 10-11 from NUB are massive, coarse-grained peridotites. Olivine is the dominant phase in these rocks. They also contain orthopyroxene, amphibole, spinel and magnetite¹⁴. The chemical composition of these samples including concentration data for highly siderophile elements and $^{187}\text{Os}/^{188}\text{Os}$ data were reported in a previous study¹⁴. Sample 10-27 is a harzburgite from the South of the Isua supracrustal belt (SOISB). The mineral assemblage of this rock is comparable to other harzburgites collected from the same locality¹⁴. These rocks are typically spinel-peridotites with harzburgitic mineral assemblages composed of mainly olivine and variable amounts of orthopyroxene, amphibole and opaque phases¹⁴. A minimum age of 3.8 Gyr for the analyzed SOISB and NUB peridotites was estimated based on field relationships to surrounding 3.8 Gyr old tonalitic gneisses and crosscutting dykes^{14,36,37}.

Two of the investigated chromitites (194856, 194857) were collected from the Ujargssuit Nunât layered intrusion³⁸. For chromitites from this locality Pt-Os model ages as old as 4.36 Gyr were reported³⁹. Samples 194882B and 19488C are chromitites from a locality close to the inland ice that most likely belongs to the same sequence as the chromitites from the Ujargssuit Nunât layered intrusion.

The dunite sample 194907 was collected from an antigorite lens located within the northeastern part of the 3.7 Gyr-old Isua supracrustal belt, which has previously been

referred to as Dunite Lens B^{40,41}. The ISB dunites also contain orthopyroxene and spinel, and very minor amounts of mostly altered clinopyroxene⁴⁰.

Two of the analyzed chromitites (186466, 186479) derive from the Seqi ultramafic complex. The major and trace element composition including concentration data for platinum-group elements of these samples were reported in a previous study⁴². The Seqi ultramafic complex represents a peridotite enclave hosted by tonalitic orthogneiss within the 3.0 Gyr-old Akia terrane. A minimum age for the ultramafic body is constrained by 2.98 Gyr-old crosscutting granitoid sheets⁴², although unpublished Re-Os isotope data show a consistent 3.1 Gyr mantle depletion age for the Seqi ultramafic complex. The highly refractory peridotites and chromitites are interpreted to represent the remnant of a fragmented layered complex or a magma conduit. The ultramafic rocks formed from a magnesian-rich near-anhydrous magma as olivine dominated cumulates with high modal contents of chromite⁴². Their parental magma was generated by high degrees of partial melting of a mantle source that likely represents the precursor of the regional sub-continental lithospheric mantle.

The chromitite sample Pil 16-61 was collected from the Warawoona Group located within the Pilbara craton. The chromitite may be as old as the associated Mount Ada basalt unit (3.5 Gyr) or it may be part of the younger 3.2 Gyr-old Dalton Suite sill complex⁴³.

The investigated komatiite rock (OKUM) from the 2.7 Gyr-old Abitibi greenstone belt (Canada) is a commercially available rock reference sample provided by the International Association of Geoanalysts.

Two chromitites (UG2, LG6) from the 2.05 Gyr-old Bushveld complex (South Africa) were used as a reference sample to validate the analytical method and to assess the precision and the accuracy of the Ru isotope measurements. The Ru isotope composition of UG-2 was previously determined employing a different digestion method (alkaline fusion)⁵.

Ruthenium separation and purification

The required amount of sample material to yield sufficient Ru for a high-precision measurement was estimated based on previously reported Ru concentrations (10-9, 10-11, UG-2, LG-6, OKUM, 186466, 186479)^{42,44,45} or Ru concentrations reported for samples of similar composition from the same locality (10-27, 194907)^{23,46}. For samples where such information was not available (e.g. 194856, 194857, Pil16-61) the Ru concentrations were determined on a 1 g powder test portion digested in a high pressure asher in reverse aqua regia (5 ml conc. HNO₃ + 2.5 ml conc. HCl). Before quantification of Ru for these samples, the digestion solution was dried down, converted twice with 5 ml of 6M HCl, taken up in 0.2 M HCl and loaded on a cation column to remove matrix elements as described below. Ruthenium concentrations were determined in the eluted Ru fractions by external calibration using a quadrupole inductively coupled plasma mass-spectrometer (ThermoScientific iCap). We note that the concentrations determined by this procedure may underestimate the actual concentration of samples because some Ru may have been lost as a volatile tetroxide (RuO₄) when the aqua regia solutions were dried down. Therefore, these concentrations are considered only as informal values. In a similar manner, the Ru contents of two chromitites (194882B, 194884C) were estimated based on a 1% sample aliquot taken after NiS digestion

and cation column chemistry as described below. However, we note that these estimates represent only informational values too because as described below the Ru yield of the NiS procedure is <100%.

For the NiS procedure powder aliquots of 5-10 g were digested using a NiS fire assay technique⁴⁷. For chromitite samples with high Ru concentrations (UG-2, LG-6, 194856, 194857, Pil16-61) one NiS digestion with 5 g of sample powder was needed to yield sufficient amounts of Ru. For ultramafic samples with lower Ru concentrations (harzburgites, dunites, komatiites, and some chromitites) multiple NiS digestions with 10 g of sample powder had to be prepared. The total number of NiS digestions and the amount of sample material used for each respective NiS bead are given in Extended Data Table 2. To each 5-10 g sample portion appropriate amounts of Ni, S, Borax and Na₂CO₃ were added and thoroughly mixed. The mixture was fluxed in a muffle furnace for 75 minutes at 1000°C. After cooling, the NiS beads were physically removed from the quenched silicate melt.

For the majority of samples, the NiS procedure resulted in about one to three cm-sized beads that could readily be recovered from the quenched silicate. The Ru yield of the NiS procedure was determined based on sample powders with well-known Ru concentrations (UG-2, OKUM, 10-9, 10-11, 186466, 186479). For these samples the Ru yield usually varied from 60-95%. However, in case of three replicate UG-2 digestions the Ru yields were only on the order of 10-20%. The lower yields resulted from incomplete homogenization and subsequent inefficient extraction of NiS beads from the quenched silicate. For these samples the NiS digestions produced finely dispersed mm- to µm-sized spherules within the quenched silicate. Careful homogenization of the NiS sample-flux mixtures before digestion helped to avoid this problem.

The NiS beads were crushed in an agate mortar, transferred into 60 ml Savillex beakers followed by the addition of 30 ml concentrated HCl. The solutions were evaporated to near dryness on a hotplate at 100°C. This step was repeated with another 30 ml of concentrated HCl and 20 ml 1 M HCl.

Ruthenium was separated from the dissolved NiS beads using cation exchange chromatography⁴⁸. Each dissolved NiS bead from a single fire assay digestion was split over three cation columns filled with 10 ml AG50 X8 resin, respectively. The resin was equilibrated with 20 ml 0.2 M HCl. Ruthenium and other platinum-group elements were loaded and eluted in 14 ml 0.2 M HCl. The eluted Ru fractions from each sample were recombined and a small aliquot (1%) was taken to determine the amount of Ru and remaining matrix elements (mainly Ni). If significant amounts of matrix elements passed through the column (if Ni/Ru > 1), the combined fractions of samples were passed for a second time over a single 10 ml cation column. The Ru yields from the cation column are usually >95%. The eluted sample solutions were dried down on a hotplate, recombined and Ru was further purified using a macro-distillation unit as described elsewhere⁴⁸. After the distillation the purified Ru fractions were dried down on a hotplate and dissolved in 0.5 ml 0.28 M HNO₃ from which a small aliquot was prepared as a predilution to determine the Ru yield and to check for potential interfering elements. The distillation yields were usually

between ~40-80%. The total Ru yield of the analytical procedure including NiS digestion, column chemistry and distillation is typically 30–70%, estimated based on samples with known Ru concentrations (UG-2, OKUM, 10-9, 10-11, 186466, 186479). In case of three UG-2 digestions the total yield was only 6-21%. Even though for these samples the yields of the distillation were 50-80%, the low total Ru yields are caused by inefficient extraction of NiS beads, as described above. However, neither the total Ru yield of the entire analytical procedure nor the respective yields from the NiS digestion or the Ru distillation have any effect on the accuracy of the Ru isotope data (Extended Data Figure 1).

The procedural blank for a single NiS digestion, including column chemistry and distillation varied between 185 and 435 pg (n=3). The blank contribution was <<1% for the majority of samples and <2% for OKUM and 194907 given that per each respective NiS digestion 30 ng of Ru were processed.

Mass spectrometry

The Ru isotope measurements were performed using a ThermoScientific Neptune Plus multicollector inductively coupled plasma mass spectrometer (MC-ICPMS) in the Institut für Geologie und Mineralogie at the University of Cologne. For the measurements, the Ru fractions were further diluted in 0.28 M HNO₃ to yield Ru solutions of 100 ng ml⁻¹. The diluted solutions were checked for the presence of interfering elements (Zr, Ni) that could affect the accuracy of the isotope data and cannot be monitored online during the measurements. The sample solutions were introduced into the mass spectrometer at an uptake rate of ~50 ul min⁻¹ using an ESI microflow PFA nebulizer attached to a Cetac Aridus II desolvator. The isotope measurements were conducted with total ion beam intensities between 8×10^{-11} and 2×10^{-10} A, obtained for 100 ng ml⁻¹ Ru sample and standard solutions using conventional Ni H-cones. The setup was optimized to yield oxide production rates <<1% (CeO/Ce). The measurements were conducted in static mode and the seven stable Ru isotopes ⁹⁶Ru, ⁹⁸Ru, ⁹⁹Ru, ¹⁰⁰Ru, ¹⁰¹Ru, ¹⁰²Ru and ¹⁰⁴Ru as well as ⁹⁷Mo and ¹⁰⁵Pd were monitored simultaneously. Each Ru isotope analysis consisted of an on-peak baseline on a solution blank (40 integrations of 4.2 s) followed by 100 integrations of 8.4 s for each sample or standard solution and typically consumed about ~90 ng Ru. Each sample analysis was bracketed by measurements of an in-house Ru standard solution (Alfa Aesar Ru). The data were internally normalized to ⁹⁹Ru/¹⁰¹Ru = 0.7450754³¹ using the exponential law to corrected for mass-dependent isotope fractionation. The isotope data are reported as $\epsilon^i\text{Ru} = (\text{Ru}^i/\text{Ru}^{101}\text{Ru}_{\text{Sample}}/\text{Ru}^i/\text{Ru}^{101}\text{Ru}_{\text{Standard}} - 1) \times 10^4$, calculated relative to the bracketing standard of each analytical session. The accuracy and precision of the Ru isotopic measurements were evaluated by replicate digestions and multiple analyses of the UG-2 chromitite (Bushveld, South Africa), which was used as reference sample. The Ru isotope data obtained for UG-2 in this study agrees well with previously reported data⁵, where a different digestion method (alkaline fusion) was used for sample decomposition. This demonstrates that the isotope data obtained by the NiS method yields accurate results. The external reproducibility (2 s.d.) obtained for a total number of 103 individual measurements from 8 replicate UG-2 digestions is $\pm 0.43 \epsilon^{96}\text{Ru}$, $\pm 0.49 \epsilon^{98}\text{Ru}$, $\pm 0.12 \epsilon^{100}\text{Ru}$, $\pm 0.16 \epsilon^{102}\text{Ru}$ and $\pm 0.30 \epsilon^{104}\text{Ru}$.

Correction for mass-dependent isotope fractionation

The exponential law is one of the most commonly used methods to correct for natural and instrumental mass-dependent isotope fractionation. For the Ru isotope measurements, one potential caveat could be that the distillation technique used to purify the Ru could induce an isotope fraction that would not follow the exponential law. This could cause apparent isotopic anomalies for a given sample as a consequence of inaccurate mass fractionation correction. The exponential law assumes that the logarithmic fractionation $\beta = \ln(r/R)$ of a given isotopic ratio is expressed as a function of the mass log-difference ($\ln M = \ln(M_2/M_1)$). Considering two isotopic ratios ($r = {}^{99}\text{Ru}/{}^{101}\text{Ru}$ and $r' = {}^{100}\text{Ru}/{}^{101}\text{Ru}$) the exponential law predicts that mass fractionation produces a linear array in a $\ln(r/r')$ plot⁴⁹. This is illustrated in Extended Data Figure 2 for the measured raw ratios of ${}^{99}\text{Ru}/{}^{101}\text{Ru}$ and ${}^{100}\text{Ru}/{}^{101}\text{Ru}$. The ratios in this figure are not corrected for mass-fractionation and are normalized to a reference ratio (R and R', respectively)³¹. If the mass fractionation experienced by the samples is accurately described by the exponential law, the ratios should fall on a linear array with a slope of ~ 0.5 . In the plot two distinct mass fractionation lines can be observed for different sessions. Importantly, the slopes for both groups of sessions are indistinguishable within error and are in very good agreement with the slope predicted by the exponential law. Most importantly, the samples purified by distillation fall on the same respective mass fractionation line as their associated Alfa Aesar bracketing standards. This clearly demonstrates that the Ru distillation does not induce any non-exponential mass-fractionation effects for the samples in comparison to the bracketing standard. This observation is also independent from the Ru yield of the samples and does not change if other Ru isotope ratios are considered. Therefore, the Ru isotope anomalies obtained for the SW Greenland samples cannot reflect inaccurate mass fractionation correction. The shift observed for samples and associated standards plotting on a distinct mass fractionation array was caused by a maintenance in May 2019 during which a Faraday cup was replaced. However, because the data are reported as relative deviations in parts per 10^4 from the Alfa Aesar bracketing standard, and because samples and bracketing standards are shifted by the same magnitude, this does not affect the accuracy of the data. This is also confirmed by replicate digestions of sample 10-9 that were analyzed in both groups of sessions. The $\epsilon^{100}\text{Ru}$ values for this sample is indistinguishable within analytical uncertainty.

An additional argument against non-exponential mass fractionation effects is that nucleosynthetic Ru isotope anomalies caused by variable contributions of s-process Ru nuclides would not cause any $\epsilon^{104}\text{Ru}$ anomalies in the ${}^{99}\text{Ru}/{}^{101}\text{Ru}$ normalization scheme. Because the $\epsilon^{104}\text{Ru}$ values for all analyzed samples fall within the external reproducibility of the method (± 0.30 for $\epsilon^{104}\text{Ru}$), this further demonstrates that sample distillation does not cause non-exponential mass fractionation effects.

Isobaric interferences

The accuracy of the Ru isotopic measurements could be compromised by isobaric interferences from Mo, Pd, Zr and Ni argide species, or potential effects related to remaining S in the analyzed sample solutions. While interferences from Mo and Pd are simultaneously monitored and corrected for during the measurements⁴⁸, this is not the case for isobars from Zr and Ni argides. Due to the design of the collector block and limited availability of

collectors, Zr and Ni could not be simultaneously monitored during the measurements. However, Zr is very effectively separated from Ru by cation exchange chemistry. Hence, all analyzed sample solutions (except for one digestion of sample 10-27) had Zr intensities indistinguishable from the background of the 0.28 M HNO₃ and the Ru standard solution. Only one analyzed sample (10-27) had slightly elevated Zr/Ru of 0.0008 and, hence, its $\epsilon^{96}\text{Ru}$ value is slightly elevated due to an isobaric interference from ^{96}Zr that could not be corrected. The Zr contained in the one analyzed sample solution most likely reflects a random contamination from the lab-ware used during sample preparation which was not observed for other samples.

In case of Ni, during the initial stage of the project, we noticed that a few processed reference samples after the cation chemistry still contained considerable amounts of Ni. For these samples, even after further purification of Ru by distillation, smaller amounts of Ni (between 1 and 10 ng ml⁻¹) were observed in the sample solutions to be analyzed. During the isotopic measurements Ni readily forms argide species in the plasma that interfere with Ru isobars⁵⁰. In order to assess potential effects from Ni argide species on the measured Ru isotope data, a 100 ng ml⁻¹ Ru standard solution was doped with varying amounts of Ni to yield concentrations between 0.2 pg ml⁻¹ and 50 ng ml⁻¹. The results of this test show that the measured Ru isotope compositions for 100 ng ml⁻¹ Ru solutions are not affected for samples with Ni/Ru ratios <0.01 (Extended Data Figure 3a,b). For sample solutions with higher amounts of Ni, positive anomalies are observed, which are most pronounced for ^{98}Ru and to a lesser extent for ^{100}Ru . Other Ru isotope masses (^{102}Ru and ^{104}Ru), owing to the lower abundance of the higher mass Ni isotopes, are not significantly affected by Ni argide species. In order to avoid any interferences from Ni argides during the isotopic measurements, the final dilutions of all samples analyzed in this study were carefully checked for their Ni contents before the analysis. The intensity of Ni, monitored with a scan on mass ^{58}Ni , in the finally diluted sample solutions was indistinguishable from the background intensity observed for the Ru solution standard and for 0.28 M HNO₃ (10–30 mV on ^{58}Ni). These negligible amounts of Ni are insignificant and have no effect on the measured data. The minimal Ni background originates from the Ni cones of the instrumental setup.

In order to eliminate any potential effects on the isotopic measurements caused by sulfur (S) in the analyzed sample solutions, the S from the crushed NiS beads was nearly quantitatively removed by evaporation as H₂S gas during dissolution of the beads with concentrated HCl. After further purification of Ru by column chemistry and distillation, the S contents in the final sample solutions were <25 ng ml⁻¹ for all analyzed samples. Tests with S-doped Alfa Aesar Ru standard solutions showed that, even if a 100 ng ml⁻¹ Ru standard solution contains large excesses of S (S/Ru = 5), the accuracy of the Ru isotope measurements is not compromised (Extended Data Figure 3c,d).

Nuclear field shift

Previous studies have shown that mass-independent Ru isotope anomalies could be caused by nuclear field shift-induced fractionation effects⁵¹. In case of meteorites and their components such effects could be a primary feature resulting from evaporation/condensation

processes in nature. However, experimental studies have shown that mass-independent effects could also be generated in the laboratory during sample preparation⁵¹. In this section we explore the potential effects from nuclear field shift-induced fractionation of Ru isotopes. These fractionations can be predicted based on differences in the mean-squared nuclear charge radii between nuclides of a given element. The resulting effects on the measured Ru isotopic composition can be calculated in ϵ -units using the following equation⁵¹:

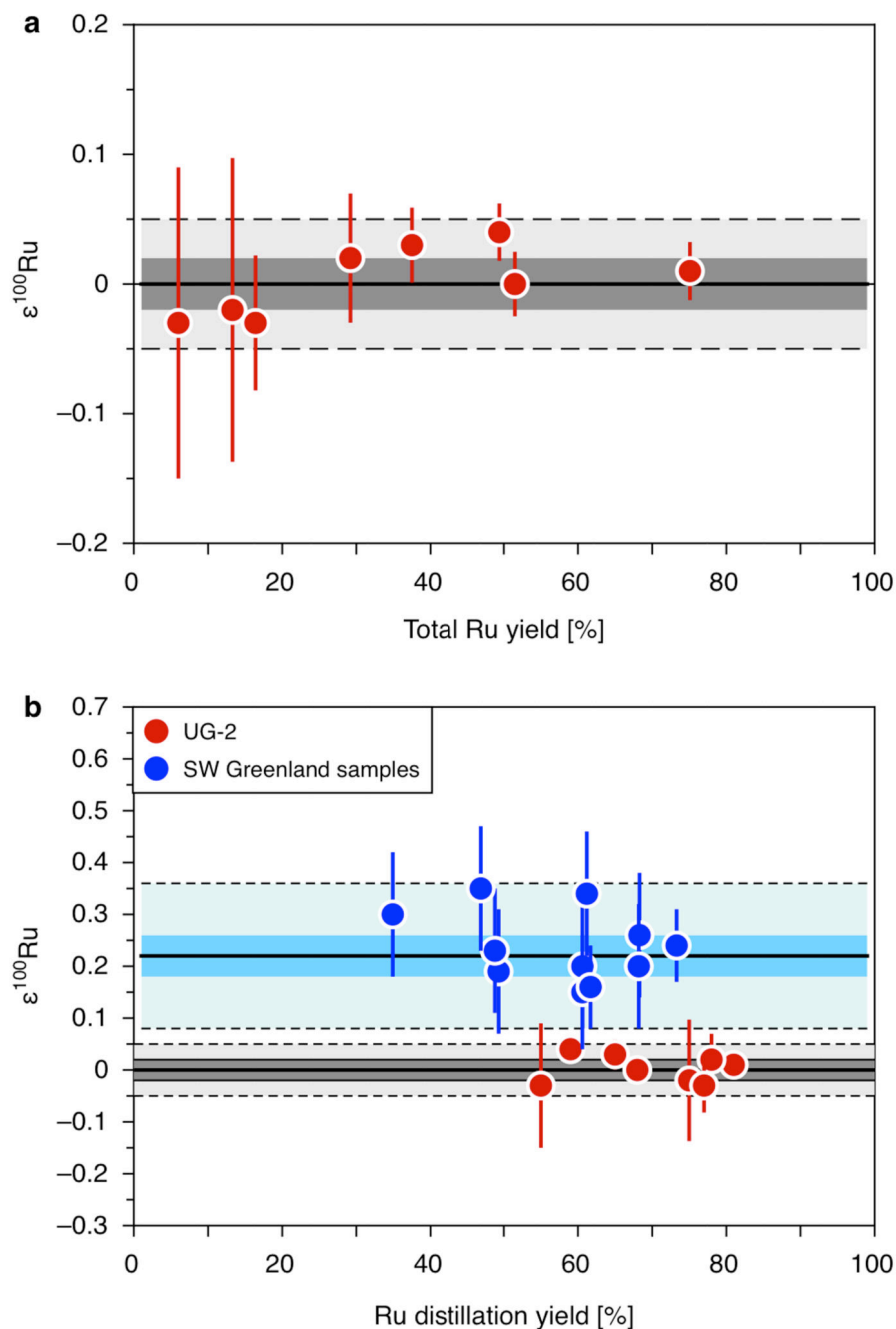
$$\epsilon_{m_i} = \left(\delta \langle r^2 \rangle_{m_1, m_i} - \frac{m_2(m_i - m_1)}{m_i(m_2 - m_1)} \delta \langle r^2 \rangle_{m_1, m_2} \right) \times \alpha$$

where m_1 and m_2 are the atomic masses of the two isotopes of an element chosen for internal normalization, m_i refers to the atomic mass of another isotope indexed with variable i , $\delta \langle r^2 \rangle$ denotes the difference in mean-squared nuclear charge radii of the respective isotope pair and α is an adjustable parameter that determines the magnitude of mass-independent fractionation, which is a function of temperature T as $1/T$. In plots of $\epsilon^{102}\text{Ru}$ and $\epsilon^{96}\text{Ru}$ vs. $\epsilon^{100}\text{Ru}$ (Extended Data Figure 4) the slopes calculated for the nuclear field shift fractionation are clearly distinct from the slope predicted by a variation in s-process Ru nuclides. The Ru isotopic compositions obtained for Eoarchean SW Greenland rocks does not plot on the calculated slope for nuclear field shift but instead plots on the s-process mixing line. As such the anomalies identified in the SW Greenland rocks cannot be explained by nuclear field shift-induced fractionation and therefore reflect isotope anomalies of nucleosynthetic origin.

Fissiogenic Ru

Spontaneous fission of uranium has been shown to produce Ru nuclides with relative abundances that are distinct from naturally occurring Ru⁵². Fissiogenic Ru primarily consists of ^{99}Ru (33.4 %), ^{101}Ru (28.9 %), ^{102}Ru (24.7 %) and ^{104}Ru (12.4 %)⁵³. The presence of an inherited fission-produced fraction of Ru in a rock sample would induce a characteristic isotope anomaly pattern that would be distinct from anomalies of nucleosynthetic or nuclear field shift origin. Because ^{96}Ru and ^{100}Ru are not a significant fission product⁵³, the presence of an inherited fraction of fissiogenic Ru in a rock sample would cause negative $\epsilon^{96}\text{Ru}$ and $\epsilon^{100}\text{Ru}$ anomalies, which are not observed for any of the analyzed samples. On the other hand, a deficit of such an inherited fissiogenic Ru component would yield positive $\epsilon^{96}\text{Ru}$ and $\epsilon^{100}\text{Ru}$ anomalies, which are also not observed. This is shown in Extended Data Figure 4b where samples with an excess or a deficit of such a fissiogenic Ru component would fall on a mixing line with a distinct slope. Hence, the isotopic composition of the samples with positive $\epsilon^{100}\text{Ru}$ anomaly cannot be explained by either an excess or a deficit of fissiogenic Ru nuclides.

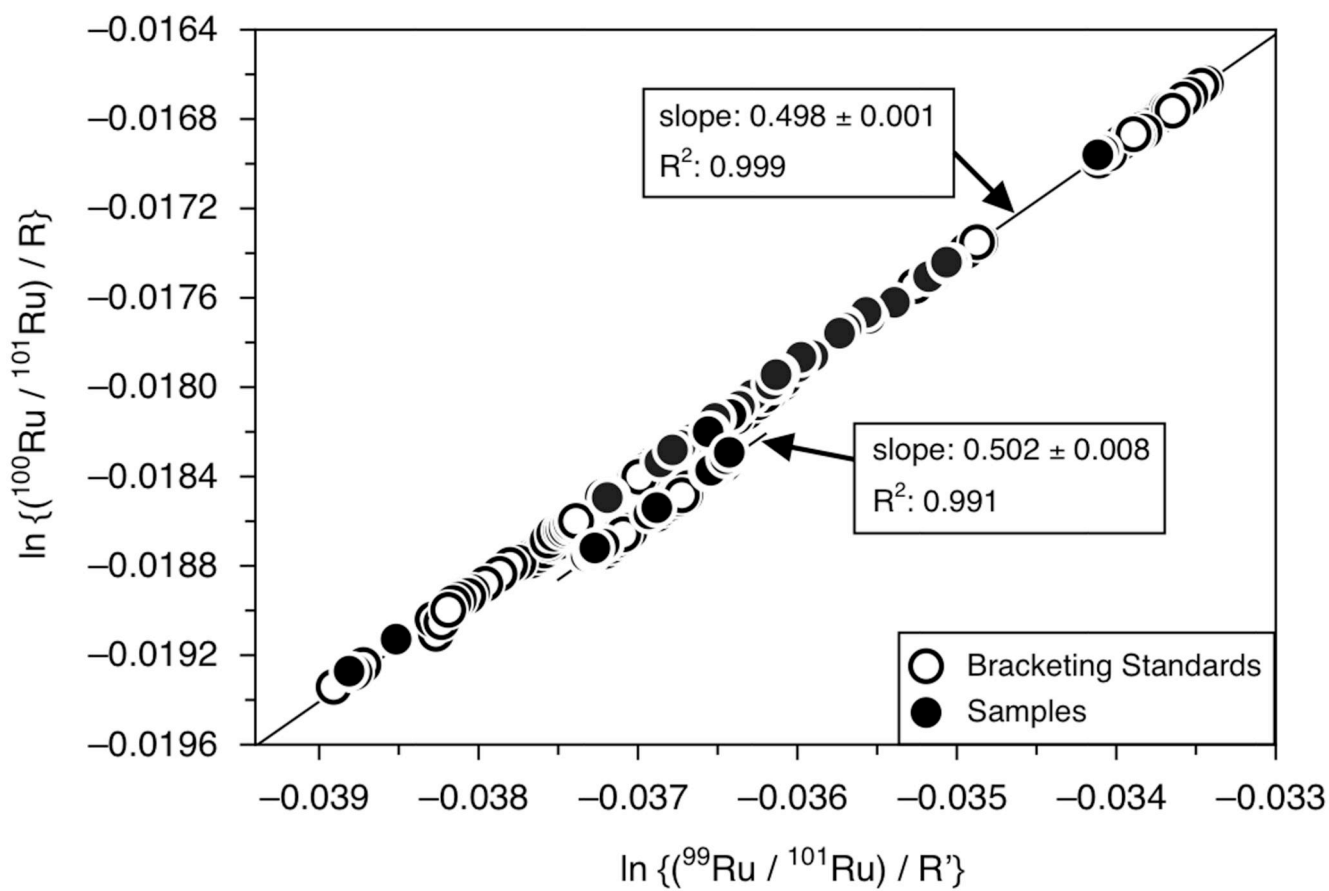
Extended Data



Extended data Figure 1. Ruthenium yields of the total analytical procedure and Ru yields from the distillation plotted against $\epsilon^{100}\text{Ru}$ data for replicate digestions of UG-2 and SW Greenland samples.

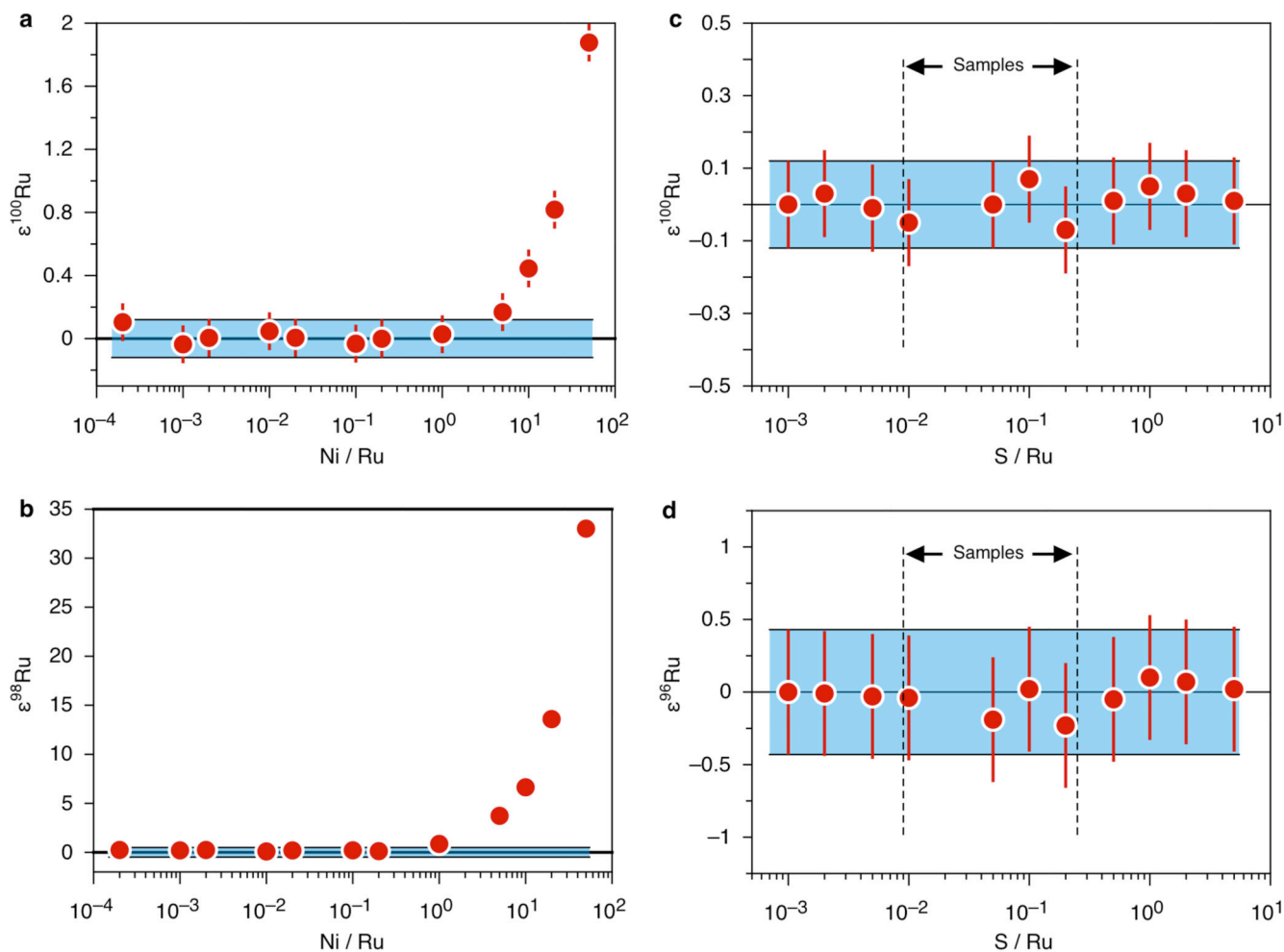
The plot shows that the accuracy of the $\epsilon^{100}\text{Ru}$ data is not affected by the Ru yield of the total analytical procedure (a) or the Ru yield of the distillation (b), respectively. The grey and blue areas represent the 95% confidence interval uncertainties, light grey and blue areas limited by dashed lines indicate the 2 s.d. uncertainty as stated for the calculated mean values of the Bushveld igneous complex and the Itsaq gneiss complex (Extended Data Table

1). Note that in **(b)** for the SW Greenland samples it was not possible to determine the Ru distillation yield for all replicates of the analyzed samples.



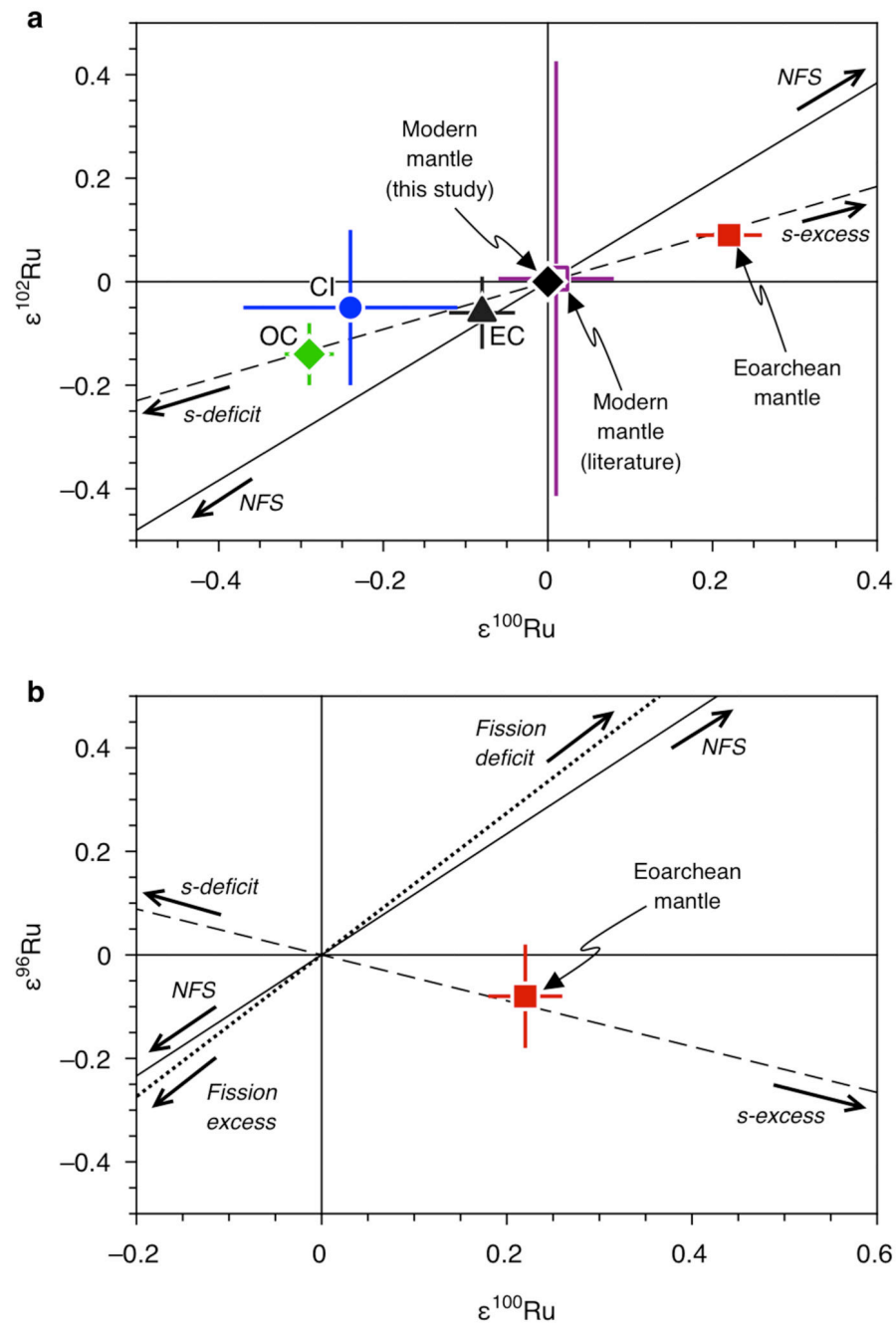
Extended data Figure 2. Ruthenium isotope plot showing the logarithmic (ln) values of the measured raw ratios for $^{99}\text{Ru}/^{101}\text{Ru}$ and $^{100}\text{Ru}/^{101}\text{Ru}$ obtained for 100 ng ml^{-1} sample solutions and associated Alfa Aesar Ru bracketing standards.

The measured isotope ratios are shown as raw ratios uncorrected for mass-dependent fractionation and are normalized to reference ratios R and R' . In the plot two distinct mass fractionation lines can be observed. The slopes for both lines are indistinguishable within error and are in very good agreement with the predicted slope of 0.5, which would be expected if the mass-dependent fractionation could accurately be corrected for by the exponential law (see Methods for details). Most importantly, the samples purified by distillation fall on the same respective mass fractionation line as their associated Alfa Aesar bracketing standards. Hence, this clearly demonstrates that the Ru distillation does not induce any unaccounted mass-fractionation effects for the samples in comparison to the bracketing standards. The shift observed for samples and associated standards plotting on a distinct mass fractionation array was caused by a maintenance on the mass spectrometer in May 2019 during which a Faraday cup was changed. However, this does not affect the accuracy of the isotopic data because the analyzed samples and their associated bracketing standards are shifted by the same magnitude, and the isotopic data are expressed as relative deviations in parts per 10^4 (ϵ values) from the bracketing standards.



Extended data Figure 3. Ruthenium isotope data obtained for ng ml^{-1} Alfa Aesar Ru standard solutions doped with variable amounts of Ni and S.

The effect of Ni argide interferences on the measured $\epsilon^{100}\text{Ru}$ (a) and $\epsilon^{98}\text{Ru}$ (b) isotopic compositions of a 100 ng ml^{-1} Ru standard solution doped with varying amounts of Ni. The accuracy of the measured isotopic compositions is not affected for samples with $\text{Ni/Ru} < 10^{-2}$. Panels (c) and (d) show that even if high amounts of S ($\text{S/Ru} = 5$) are present in the analyzed sample solutions, this has no effect on the accuracy of the measured $\epsilon^{100}\text{Ru}$ and $\epsilon^{96}\text{Ru}$ data. Vertical dashed lines in (c) and (d) indicate the range of S/Ru of the analyzed samples. The blue areas in (a-d) indicate the external reproducibility of the method as defined by the standard deviation (2 s.d.) of replicate digestions and repeated analysis of the UG-2 reference sample (see Methods).



Extended data Figure 4. Ruthenium isotope plots illustrating systematic compositional differences between enstatite (EC), ordinary (OC) and CI carbonaceous chondrites (CI), modern mantle and pre-late veneer mantle in comparison to mixing lines calculated between the modern mantle composition and isotopic variations caused by variable contributions of s-process Ru nuclides, a fissionogenic Ru component, and variations of nuclear field-shift induced isotope fractionations.

(a) Ruthenium isotope data for the Eoarchean mantle of SW Greenland, the modern mantle, and ordinary, enstatite and CI carbonaceous chondrites in comparison to a mixing line calculated between the composition of the modern mantle ($\epsilon^{102}\text{Ru} = \epsilon^{100}\text{Ru} = 0$) and an s-process component³⁴ (dashed line), and the slope calculated for a nuclear field shift-induced

(NSF) fractionation⁵¹ (black solid line). **(b)** Ruthenium isotope composition of the Eoarchean mantle in comparison to mixing lines calculated between the composition of the modern mantle ($e^{96}\text{Ru} = e^{100}\text{Ru} = 0$) and a fissiogenic Ru component⁵³ (dotted line), an *s*-process component³⁴ (dashed line), and the slope calculated for nuclear field shift-induced (NSF) isotope fraction⁵¹ (solid black line).

Extended Data Table 1
Ruthenium isotope data for ultramafic rocks

Sample*	Rock [†]	n [‡]	$e^{96}\text{Ru}^{\S}$	±	$e^{98}\text{Ru}^{\S}$	±	$e^{100}\text{Ru}^{\S}$	±	$e^{102}\text{Ru}^{\S}$	±	$e^{104}\text{Ru}^{\S}$	±
Greenland												
Itsaq gneiss complex (IGC)												
<i>Narssaq ultramafic body (NUB), 3.8 Gyr</i>												
10_9	H	1	0.13	0.43	-0.04	0.49	0.19	0.12	0.10	0.16	0.17	0.30
replicate	H	2	0.28	0.43	0.42	0.49	0.30	0.12	0.13	0.16	-0.01	0.30
10_11	D	2	-0.07	0.43	0.29	0.49	0.34	0.12	0.08	0.16	-0.10	0.30
<i>South of the Isua supracrustal belt (SOISB), 3.8 Gyr</i>												
10_27	H	1	(1.19) [¶]	0.43	0.33	0.49	0.23	0.12	0.03	0.16	0.04	0.30
replicate		1	0.03	0.43	0.58	0.49	0.23	0.12	0.18	0.16	0.00	0.30
<i>Ujaragssuit Nunât complex, 3.8 Gyr</i>												
194856	Chr	6	-0.04	0.20	0.18	0.17	0.17	0.09	0.06	0.06	-0.10	0.08
replicate		5	-0.27	0.29	0.04	0.35	0.15	0.11	0.07	0.04	-0.03	0.13
replicate		3	-0.25	0.43	0.40	0.49	0.35	0.12	0.13	0.16	-0.11	0.30
194857	Chr	10	-0.20	0.09	0.06	0.18	0.19	0.03	0.12	0.06	0.00	0.08
replicate		5	-0.17	0.22	0.17	0.31	0.16	0.08	0.06	0.17	-0.08	0.16
replicate		11	-0.09	0.20	0.10	0.18	0.13	0.04	0.05	0.05	-0.11	0.11
194882B	Chr	3	0.03	0.43	0.30	0.49	0.19	0.12	0.07	0.16	0.13	0.30
194884C	Chr	7	-0.17	0.11	0.06	0.14	0.24	0.07	0.09	0.09	-0.08	0.09
<i>Isua supracrustal belt (ISB), 3.7 Gyr</i>												
194907	D	1	-0.23	0.43	0.24	0.49	0.26	0.12	0.10	0.16	-0.20	0.30
Mean IGC (n=14) ^{¶¶}			-0.08	0.1	0.22	0.10	0.22	0.04	0.09	0.02	-0.03	0.06
2 s.d. _{IGC} ^{¶¶}				0.33		0.35		0.14		0.08		0.20
<i>Seqi ultramafic complex, >3.0 Gyr</i>												
186466	Chr	2	-0.44	0.43	-0.10	0.49	0.20	0.12	0.04	0.16	-0.29	0.30
replicate		2	-0.14	0.43	0.60	0.49	0.13	0.12	0.04	0.16	-0.13	0.30
186479	Chr	3	0.10	0.43	0.30	0.49	0.20	0.12	0.08	0.16	-0.17	0.30
Australia												
Pilbara craton, Warawoona Group, 3.5-3.2 Gyr												
Pil 16-61	Chr	3	-0.03	0.43	-0.11	0.49	0.05	0.12	0.01	0.16	-0.02	0.30
replicate		3	-0.25	0.43	-0.17	0.49	0.05	0.12	-0.06	0.16	-0.05	0.30
Canada												

Sample*	Rock [†]	n [‡]	$\epsilon^{96}\text{Ru}^{\S}$	\pm	$\epsilon^{98}\text{Ru}^{\S}$	\pm	$\epsilon^{100}\text{Ru}^{\S}$	\pm	$\epsilon^{102}\text{Ru}^{\S}$	\pm	$\epsilon^{104}\text{Ru}^{\S}$	\pm
Abitibi greenstone belt, 2.7 Gyr												
OKUM	Kom	1	0.24	0.43	0.58	0.49	0.07	0.12	-0.03	0.16	0.08	0.30
South Africa												
Bushveld igneous complex, 2.05 Gyr												
UG-2	Chr	20	-0.12	0.08	-0.06	0.10	0.00	0.02	0.03	0.04	0.05	0.07
replicate		29	-0.12	0.08	0.03	0.08	0.01	0.02	-0.01	0.03	-0.06	0.06
replicate		19	-0.11	0.10	0.13	0.11	0.04	0.02	0.04	0.04	0.05	0.07
replicate		11	-0.11	0.15	0.18	0.11	0.02	0.05	0.01	0.04	-0.02	0.10
replicate		5	-0.08	0.47	-0.19	0.44	-0.02	0.12	-0.02	0.11	0.06	0.23
replicate		2	-0.15	0.43	-0.34	0.49	-0.03	0.12	-0.03	0.16	0.08	0.30
replicate		6	-0.31	0.25	0.13	0.31	-0.03	0.05	-0.02	0.07	0.08	0.10
replicate		11	0.02	0.12	-0.01	0.16	0.03	0.03	-0.02	0.05	-0.04	0.09
LG-6	Chr	4	-0.20	0.28	0.05	0.32	0.01	0.09	-0.01	0.09	-0.04	0.18
Mean Bushveld (n=9) [¶]			-0.13	0.07	-0.01	0.13	0.00	0.02	0.00	0.02	0.02	0.04
2 s.d. Bushveld ^{//}				0.18		0.33		0.05		0.05		0.12

* H: harzburgite, D: dunite, Chr: chromitite, Kom: komatiite.

[†] Ruthenium concentrations reported for the same samples or samples from the same locality. Italicized values indicate Ru concentrations determined in this study as described in methods section.

[‡] Number of individual NiS digestions (n) and amount of sample material (in g) taken for each single NiS digestion processed for each sample and replicate sample analysis. In cases where different numbers of NiS digestions were processed for a replicate sample analysis this is indicated by the number in parenthesis. If not stated otherwise the same number of NiS digestions was used for all replicates.

[§] Re-Os isotope data reported for the same samples or for samples of similar composition from the same locality. Note that the different ranges reported for chromitite samples from the Ujaragssuit Nunat complex were not obtained for the same samples and represent data reported by different previous studies for chromitites from the same locality or sampling area.

^{//} Age used for calculation of the initial $^{187}\text{Os}/^{188}\text{Os}$ isotope composition as quoted in literature.

[¶] Initial $^{187}\text{Os}/^{188}\text{Os}$ isotope composition calculated at the time of emplacement of the samples.

[#] γOs values refer to the relative deviation in % of the calculated initial $^{187}\text{Os}/^{188}\text{Os}$ isotope compositions of samples relative to the chondritic Os isotope composition at the time of emplacement of the samples.

** References for Ru concentration and Os isotope data.

Extended Data Table 2 Ruthenium concentration data, details about the NiS procedure and Re-Os isotope data for ultramafic rocks

Sample	Rock*	Ru (ng g ⁻¹) [†]	NiS n x (g) [‡]	$^{187}\text{Os}/^{188}\text{Os}^{\S}$	$^{187}\text{Re}/^{188}\text{Os}^{\S}$	Age (Gyr)	$^{187}\text{Os}/^{188}\text{Os}_{\text{ini}}^{\¶}$	$\gamma\text{Os}^{\#}$	Ref.**
Greenland									
Itsaq gneiss complex (IGC)									
<i>Narssaq ultramafic body (NUB), 3.8 Gyr</i>									
10_9	H	7.76	5 (8) x10g	0.1013	0.044	3.80	0.09845	-2.3	14

Sample	Rock*	Ru (ng g ⁻¹) [†]	NiS n x _g [‡] (g) [‡]	¹⁸⁷ Os/ ¹⁸⁸ Os [§]	¹⁸⁷ Re/ ¹⁸⁸ Os [§]	Age (Gyr)	¹⁸⁷ Os/ ¹⁸⁸ Os _{ini.} [¶]	yOs [#]	Ref.**
10_11	D	8.27	8 x10g	0.1013	0.042	3.80	0.09857	-2.2	14
<i>South of the Isua supracrustal belt (SOISB), 3.8 Gyr</i>									
10_27	H	3.13 - 6.80	5(6) x10g	0.1010-0.1153	0.023 - 0.233	3.81	0.09942 - 0.10002	-5.3 to +5.8	14
<i>Ujaragssuit Nunât complex, 3.8 Gyr</i>									
194856	Chr	215	1 x5g	0.10471 - 0.10493	0.0008-0.0013	3.81	0.1046-0.1047	+3.9 to +4.0	33
194857	Chr	189	1 x5g	0.10490 - 0.10809	0.01424 - 0.02906	3.90	0.10395 - 0.10614	+3.9 to +6.1	38
194882B	Chr	12	6 x10g	0.104842 - 0.105590					39
194884C	Chr	23	4 x10g						
<i>Isua supracrustal belt (ISB), 3.7 Gyr</i>									
194907	D	2.43-7.06	7 x10g	0.10899 - 0.37064	0.049 - 2.96	3.80	0.1045-0.1772	+3.8 to +76.2	23
		2.9-5.3		0.10245 - 0.13411	0.042 - 0.707	3.70	0.089-0.101	-12.8 to +0.2	46
<i>Seqi ultramafic complex, >3.0 Gyr</i>									
186466	Chr	53.83	2 x5g						42
186479	Chr	53.54	2 x5g						42
Australia									
<i>Pilbara craton, Warawoona Group, 3.5-3.2 Gyr</i>									
Pil 16-61	Chr	115	1 x5g	0.10517 - 0.11926	0.0281 - 0.1688	3.46	0.0979 - 0.1130	-5.2 to +9.6	33
Canada									
<i>Abitibi greenstone belt, 2.7 Gyr</i>									
OKUM	Kom	4.25	4 x10g	0.269					44, 54
South Africa									
<i>Bushveld igneous complex, 2.05 Gyr</i>									
UG-2	Chr	760	1 x5g	0.1483 - 0.1489	0.0916				45, 55
LG-6	Chr	270 - 430	1 x5g	0.1254-0.1265	0.101 -0.117				45, 55

* The term 'replicate' indicates that the Ru isotope data were obtained for a replicate digestion of the same sample powder.

† H: harzburgite, D: dunite, Chr: chromitite, Kom: komatiite.

‡ Number of analysis of the same sample solution.

[§]Ruthenium isotope data are internally normalized to ⁹⁹Ru/¹⁰¹Ru using the exponential law and are reported as *e*-unit (0.01%) deviations from the terrestrial bracketing standard: $e^i\text{Ru} = ({}^i\text{Ru}/{}^{101}\text{Ru}_{\text{Sample}} / {}^i\text{Ru}/{}^{101}\text{Ru}_{\text{Standard}} - 1) \cdot 10^4$, where *i* = 96, 98, 100, 102 or 104. For samples measured *n* < 4 times quoted errors reflect the external uncertainty as defined by the standard deviation (2 s.d.) of replicate digestions and repeated analysis of a reference sample (see Methods). Uncertainties for samples measured *n* = 4 times are given as 95% confidence intervals of the mean calculated as:

$$(\text{s.d.} \times t_{0.95, n-1}) / \sqrt{n}.$$

[¶]Calculated averages for samples from Itsaq and Bushveld with 95% confidence interval uncertainties calculated as:

$$(\text{s.d.} \times t_{0.95, n-1}) / \sqrt{n} \text{ and } 2 \text{ s.d. uncertainties.}$$

^{¶¶}Elevated ⁹⁶Ru value due to an isobaric Zr interference that could not be corrected during the isotopic measurement (see Methods). Consequently, this value was not included for the calculation of the IGC mean value.

Extended Data Table 3
Parameter for mixing model shown in Figure 3 and
resulting ^{e100}Ru values for pre-late veneer mantle
endmember composition

	^{e100} Ru	±	Ru (ng g ⁻¹)	^{e100} Ru in pre-LV mantle	^{e100} Ru in pre-LV mantle min	^{e100} Ru in pre-LV mantle max
Chondrite groups						
Enstatite	-0.08	0.04	818 ^{§6}	0.31	0.16	0.47
Ordinary	-0.29	0.03	882 ^{§6}	1.14	1.02	1.26
Carbonaceous average	-0.90	0.61	838 ^{§6}	3.56	1.19	4.74
Carbonaceous average	-0.90	0.12	838 ^{§6}	3.56	3.08	4.03
CI	-0.24	0.13	637.4 ^{§6}	1.00	0.46	1.55
CM	-0.69	0.38	817 ^{§6}	2.90	1.30	4.49
Terrestrial mantle						
Modern mantle [*]	0.00	0.02	7.0 ¹⁶			
Eoarchean SW Greenland mantle [†]	0.22	0.04				
Pre-late veneer mantle			1.4			

^{*}The composition of the modern mantle corresponds to the mean value calculated for samples from the Bushveld complex (Extended Data Table 1).

[†]The Eoarchean SW Greenland mantle composition represents the mean value calculated for samples from the Itsaq gneiss complex (Extended Data Table 1).

Acknowledgements

We thank F. Wombacher and A. Katzemich for support in the lab and Ken Tani and Ikuya Nishio for help during field work. We acknowledge the comments of two anonymous reviewers that helped to improve the paper. This research was supported through DFG grant FI 1704/5-1 within the priority program SPP 1833 'Building a Habitable Earth' to M.F.-G., by the European Commission through ERC grant no. 669666 'Infant Earth' to C.M., by the Carlsberg Foundation grant CF18-0090 to K.S., and by Kanazawa University "SAKIGAKE 2018" to T.M. H.S. publishes with the permission of the Executive Director, Geological Survey of Western Australia.

References

- Alexander CM, et al. The provenances of asteroids, and their contributions to the volatile inventories of the terrestrial planets. *Science*. 2012; 337:721–723. [PubMed: 22798405]
- Braukmüller N, Wombacher F, Funk C, Münker C. Earth's: volatile element depletion pattern inherited from a carbonaceous chondrite-like source. *Nature Geoscience*. 2019; 12:564–568.

3. Marty B. The origins and concentrations of water, carbon, nitrogen and noble gases on Earth. *Earth and Planetary Science Letters*. 2012; 313–314:56–66.
4. Peslier AH, Schönbachler M, Busemann H, Karato S-I. Water in the Earth's Interior: Distribution and Origin. *Space Science Reviews*. 2017; 212:743–810.
5. Fischer-Gödde M, Kleine T. Ruthenium isotopic evidence for an inner Solar System origin of the late veneer. *Nature*. 2017; 541:525–527. [PubMed: 28128236]
6. Albarede F. Volatile accretion history of the terrestrial planets and dynamic implications. *Nature*. 2009; 461:1227–1233. [PubMed: 19865163]
7. Schonbachler M, Carlson RW, Horan MF, Mock TD, Hauri EH. Heterogeneous accretion and the moderately volatile element budget of Earth. *Science*. 2010; 328:884–887. [PubMed: 20466929]
8. Budde G, Burkhardt C, Kleine T. Molybdenum isotopic evidence for the late accretion of outer Solar System material to Earth. *Nature Astronomy*. 2019; 3:736–741.
9. Wang Z, Becker H. Ratios of S, Se and Te in the silicate Earth require a volatile-rich late veneer. *Nature*. 2013; 499:328–331. [PubMed: 23868263]
10. Varas-Reus MS, König S, Yierpan A, Lorrain J-P, Schoenberg R. Selenium isotopes trace a late volatile contribution to Earth from the outer Solar System. *Nature Geoscience*. 2019; 12:779–782.
11. Dauphas N. The isotopic nature of the Earth's accreting material through time. *Nature*. 2017; 541:521–524. [PubMed: 28128239]
12. Bermingham KR, Walker RJ. The ruthenium isotopic composition of the oceanic mantle. *Earth and Planetary Science Letters*. 2017; 474:466–473. [PubMed: 30956285]
13. Rubie DC, et al. Highly siderophile elements were stripped from Earth's mantle by iron sulfide segregation. *Science*. 2016; 353:1141–1144. [PubMed: 27609889]
14. van de Löcht J, et al. Earth's oldest mantle peridotites show entire record of late accretion. *Geology*. 2018; 46:199–202.
15. Brenan JM, McDonough WF. Core formation and metal-silicate fractionation of osmium and iridium from gold. *Nature Geoscience*. 2009; 2:798–801.
16. Becker H, et al. Highly siderophile element composition of the Earth's primitive upper mantle: Constraints from new data on peridotite massifs and xenoliths. *Geochimica et Cosmochimica Acta*. 2006; 70:4528–4550.
17. Chou CL. Fractionation of siderophile elements in the Earth's upper mantle. *Proc Lunar Planet Sci Conf*. 1978; 9:219–230.
18. Walker RJ. Highly siderophile elements in the Earth, Moon and Mars: Update and implications for planetary accretion and differentiation. *Chemie der Erde - Geochemistry*. 2009; 69:101–125.
19. Bermingham KR, Worsham EA, Walker RJ. New insights into Mo and Ru isotope variation in the nebula and terrestrial planet accretionary genetics. *Earth and Planetary Science Letters*. 2018; 487:221–229. [PubMed: 30880823]
20. Willbold M, Mojzsis SJ, Chen HW, Elliott T. Tungsten isotope composition of the Acasta Gneiss Complex. *Earth and Planetary Science Letters*. 2015; 419:168–177.
21. Willbold M, Elliott T, Moorbath S. The tungsten isotopic composition of the Earth's mantle before the terminal bombardment. *Nature*. 2011; 477:195–198. [PubMed: 21901010]
22. Maier WD, et al. Progressive mixing of meteoritic veneer into the early Earth's deep mantle. *Nature*. 2009; 460:620–623.
23. Dale CW, Kruijer TS, Burton KW. Highly siderophile element and ^{182}W evidence for a partial late veneer in the source of 3.8 Ga rocks from Isua, Greenland. *Earth and Planetary Science Letters*. 2017; 458:394–404.
24. Marchi S, Canup RM, Walker RJ. Heterogeneous delivery of silicate and metal to the Earth by large planetesimals. *Nature Geoscience*. 2018; 11:77–81.
25. Touboul M, Puchtel IS, Walker RJ. ^{182}W evidence for long-term preservation of early mantle differentiation products. *Science*. 2012; 335:1065–1069. [PubMed: 22345398]
26. Rizo H, et al. Preservation of Earth-forming events in the tungsten isotopic composition of modern flood basalts. *Science*. 2016; 352:809–812. [PubMed: 27174983]
27. Mundl A, et al. Tungsten-182 heterogeneity in modern ocean island basalts. *Science*. 2017; 356:66–69. [PubMed: 28386009]

28. Touboul M, Liu J, O'Neil J, Puchtel IS, Walker RJ. New insights into the Hadean mantle revealed by ^{182}W and highly siderophile element abundances of supracrustal rocks from the Nuvvuagittuq Greenstone Belt, Quebec, Canada. *Chemical Geology*. 2014; 383:63–75.
29. Tusch J, et al. Uniform ^{182}W isotope compositions in Eoarchean rocks from the Isua region, SW Greenland: The role of early silicate differentiation and missing late veneer. *Geochimica et Cosmochimica Acta*. 2019; 257:284–310.
30. Rizo H, et al. ^{182}W evidence for core-mantle interaction in the source of mantle plumes. *Geochemical Perspectives Letters*. 2019; 11:6–11.
31. Chen JH, Papanastassiou DA, Wasserburg GJ. Ruthenium endemic isotope effects in chondrites and differentiated meteorites. *Geochimica et Cosmochimica Acta*. 2010; 74:3851–3862.
32. Szilas K, Kelemen PB, Rosing MT. The petrogenesis of ultramafic rocks in the >3.7Ga Isua supracrustal belt, southern West Greenland: Geochemical evidence for two distinct magmatic cumulate trends. *Gondwana Research*. 2015; 28:565–580.
33. Bennett VC, Nutman AP, Esat TM. Constraints on mantle evolution from $^{187}\text{Os}/^{188}\text{Os}$ isotopic compositions of Archean ultramafic rocks from southern West Greenland (3.8 Ga) and Western Australia (3.46 Ga). *Geochim Cosmochim Acta*. 2002; 66:2615–2630.
34. Savina MR, et al. Extinct technetium in silicon carbide stardust grains: implications for stellar nucleosynthesis. *Science*. 2004; 303:649–652. [PubMed: 14752154]
35. Nutman AP, McGregor VR, Friend CRL, Bennett VC, Kinny PD. The Itsaq Gneiss Complex of southern West Greenland; the world's most extensive record of early crustal evolution (3900-3600 Ma). *Precambrian Research*. 1996; 78:1–39.
36. Friend C, Bennett V, Nutman A. Abyssal peridotites >3,800 Ma from southern West Greenland: field relationships, petrography, geochronology, whole-rock and mineral chemistry of dunite and harzburgite inclusions in the Itsaq Gneiss Complex. *Contributions to Mineralogy and Petrology*. 2002; 143:71–92.
37. Nutman, AP, Friend, CRL, Horie, K, Hidaka, H. *Developments in Precambrian Geology*. van Kranendonk, Martin J, Hugh Smithies, R, Bennett, Vickie C, editors. Vol. 15. Elsevier; 2007. 187–218.
38. Rollinson H, Appel PWU, Frei R. A Metamorphosed, Early Archaean Chromitite from West Greenland: Implications for the Genesis of Archaean Anorthositic Chromitites. *Journal of Petrology*. 2002; 43:2143–2170.
39. Coggon JA, Luguet A, Nowell GM, Appel PWU. Hadean mantle melting recorded by southwest Greenland chromitite ^{186}Os signatures. *Nature Geoscience*. 2013; 6:871–874.
40. Friend CRL, Nutman AP. Eoarchean ophiolites? New evidence for the debate on the Isua supracrustal belt, southern West Greenland. *American Journal of Science*. 2010; 310:826–861.
41. Friend CRL, Nutman AP. Dunites from Isua, Greenland: A ca. 3720 Ma window into subcrustal metasomatism of depleted mantle. *Geology*. 2011; 39:663–666.
42. Szilas K, et al. Highly refractory Archaean peridotite cumulates: Petrology and geochemistry of the Seqi Ultramafic Complex, SW Greenland. *Geoscience Frontiers*. 2018; 9:689–714.
43. Van Kranendonk MJ, Hugh Smithies R, Hickman AH, Wingate MTD, Bodorkos S. Evidence for Mesoarchean (~3.2 Ga) rifting of the Pilbara Craton: The missing link in an early Precambrian Wilson cycle. *Precambrian Research*. 2010; 177:145–161.
44. Savard D, Barnes S-J, Meisel T. Comparison between nickel-sulfur fire assay Te co-precipitation and isotope dilution with high-pressure asher acid digestion for the determination of platinum-group elements, rhenium and gold. *Geostandards and Geoanalytical Research*. 2010; 34:281–291.
45. Kaufmann FED, et al. Variations in composition, texture, and platinum group element mineralization in the Lower Group and Middle Group chromitites of the Northwestern Bushveld Complex, South Africa. *Economic Geology*. 2019; 114:569–590.
46. Rizo H, et al. Early Earth differentiation investigated through ^{142}Nd , ^{182}W , and highly siderophile element abundances in samples from Isua, Greenland. *Geochimica et Cosmochimica Acta*. 2016; 175:319–336.
47. Rehkämper M, Halliday AN. Development and application of new ion-dash-exchange techniques for the separation of the platinum group and other siderophile elements from geological samples. *Talanta*. 1997; 44:663–672. [PubMed: 18966788]

48. Fischer-Gödde M, Burkhardt C, Kruijer TS, Kleine T. Ru isotope heterogeneity in the solar protoplanetary disk. *Geochimica et Cosmochimica Acta*. 2015; 168:151–171.
49. Maréchal CN, Télouk P, Albarède F. Precise analysis of copper and zinc isotopic compositions by plasma-source mass spectrometry. *Chemical Geology*. 1999; 156:251–273.
50. Becker JS, Seifert G, Saprykin AI, Dietze H-J. Mass spectrometric and theoretical investigations into the formation of argon molecular ions in plasma mass spectrometry. *Journal of Analytical Atomic Spectrometry*. 1996; 11:643–648.
51. Fujii T, Moynier F, Telouk P, Albarede F. Mass-Independent isotope fractionation of molybdenum and ruthenium and the origin of isotopic anomalies in Murchison. *The Astrophysical Journal*. 2006; 647:1506–1516.
52. Hidaka H, Masuda A. Isotopic search for spontaneous fission-produced ruthenium, silver and tellurium in uraninite. *Chemical Geology*. 1993; 106:187–195.
53. Hidaka H, Holliger P. Geochemical and neutronic characteristics of the natural fossil fission reactors at Oklo and Bangombé, Gabon. *Geochimica et Cosmochimica Acta*. 1998; 62:89–108.
54. Chen K, et al. Platinum-group element abundances and Re–Os isotopic systematics of the upper continental crust through time: Evidence from glacial diamictites. *Geochimica et Cosmochimica Acta*. 2016; 191:1–16.
55. Schoenberg R, Kruger FJ, Nägler TF, Meisel T, Kramers JD. PGE enrichment in chromitite layers and the Merensky Reef of the western Bushveld Complex; a Re–Os and Rb–Sr isotope study. *Earth and Planetary Science Letters*. 1999; 172:49–64.
56. Day JMD, Brandon AD, Walker RJ. Highly siderophile elements in Earth, Mars, the Moon, and asteroids. *Reviews in Mineralogy and Geochemistry*. 2016; 81:161–238. [PubMed: 30853859]

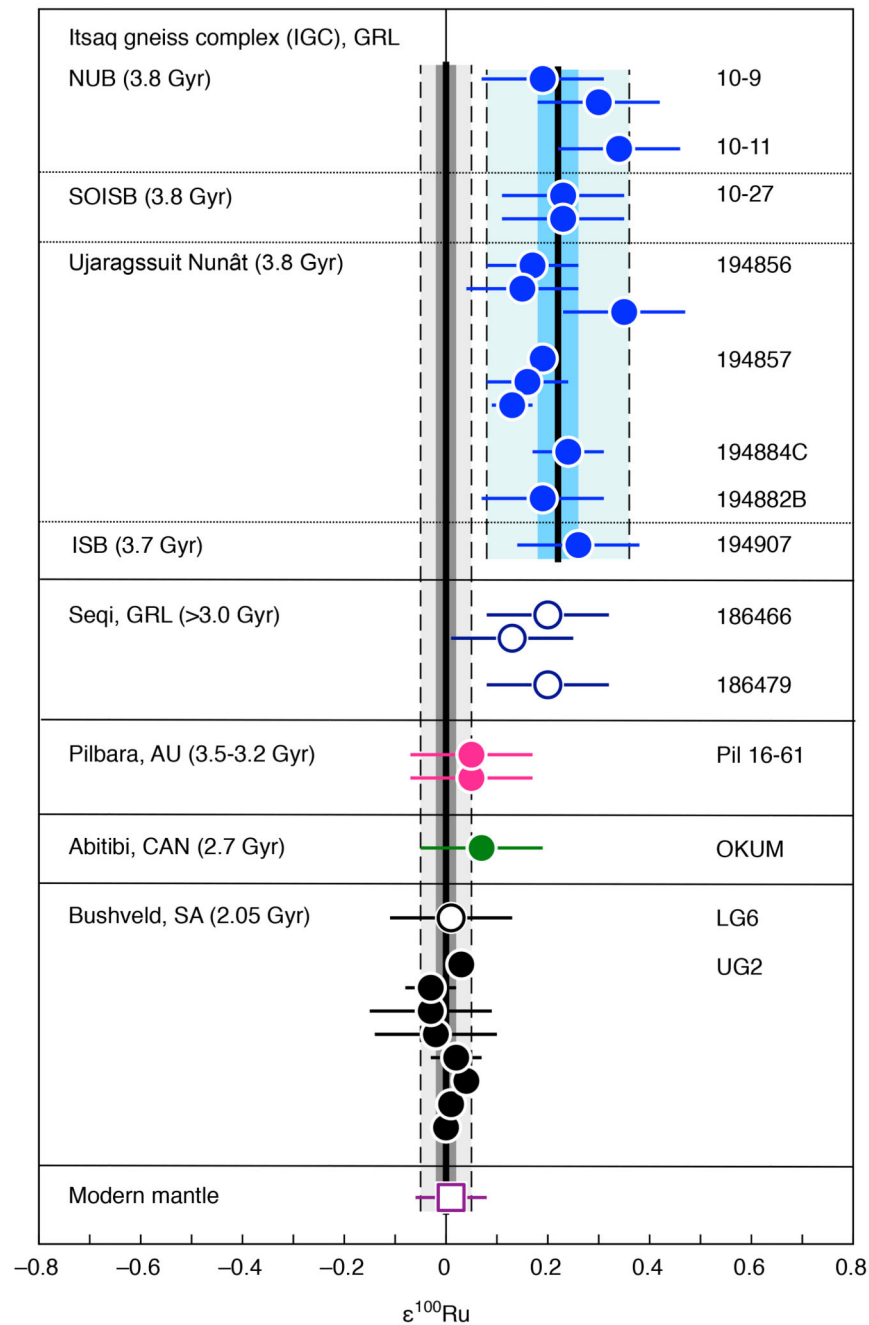


Figure 1. $\epsilon^{100}\text{Ru}$ data for Archean and Paleoproterozoic rocks, the modern mantle and chondrites.

Shown are the individual results for all analyzed samples (Extended data Table 1) in comparison to the composition of the modern mantle¹². The uncertainties for individual data points reflect the external uncertainty of the method (2 s.d. for samples measured $n < 4$ times) or 95% confidence intervals of replicate analyses of a given sample (if $n \geq 4$). The mean values for 3.8–3.7 Gyr-old Eoarchean samples from the Itsaq gneiss complex (IGC) in SW Greenland (NUB: Narssaq ultramafic body; SOISB: south of Isua supracrustal belt; ISB: Isua supracrustal belt; Ujaragssuit Nunât layered intrusion) and chromitite samples from the

Bushveld complex are shown as a solid vertical line. The darker grey and blue areas represent the respective 95% confidence interval uncertainties. Light grey and blue areas limited by dashed lines indicate the 2 s.d. uncertainty of the mean values. The uncertainty for the modern mantle composition is 2 s.d.¹².

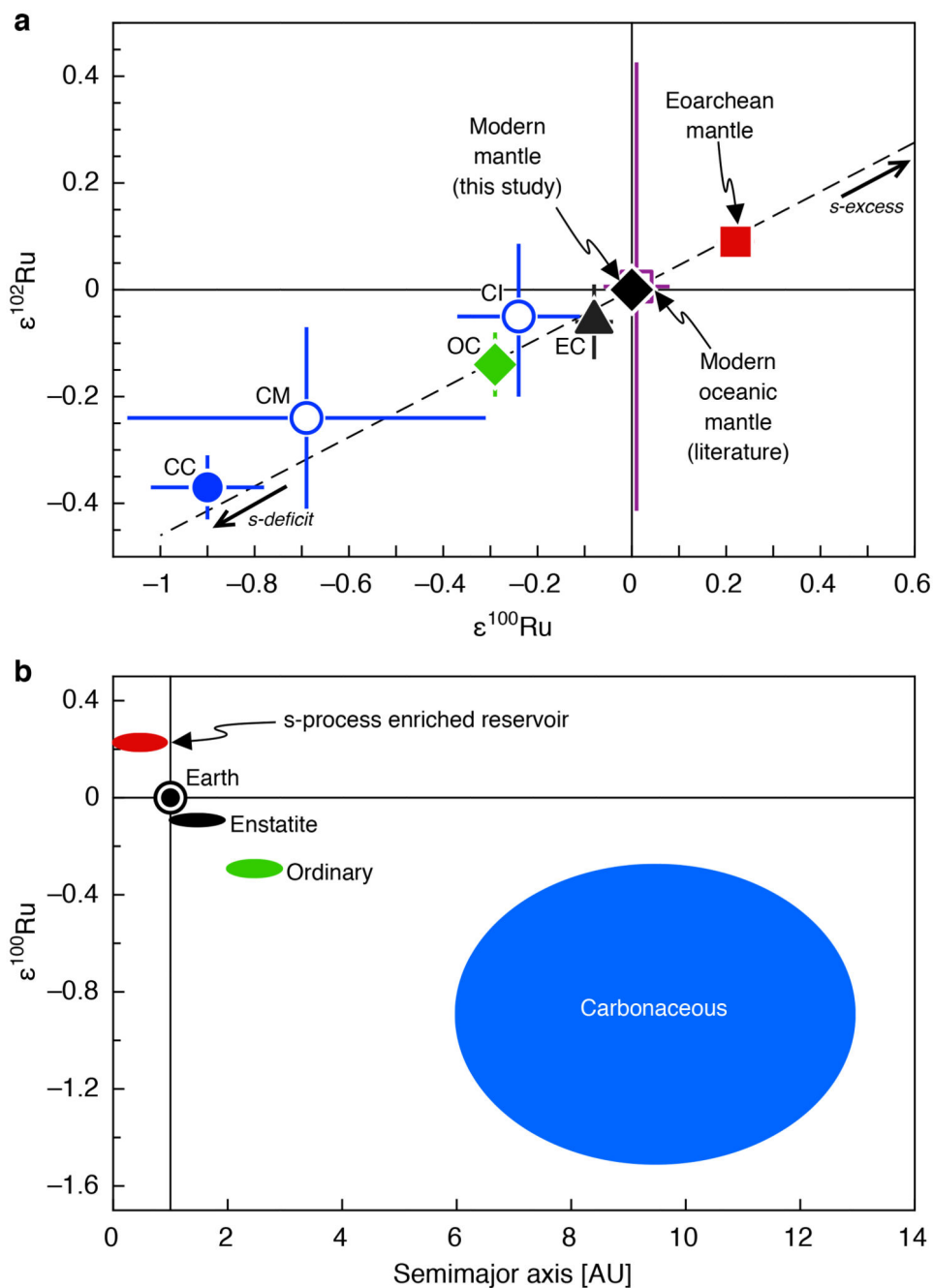


Figure 2. Ruthenium isotope plot illustrating compositional differences between enstatite (EC), ordinary (OC), average carbonaceous (CC), CI and CM carbonaceous chondrites, modern mantle and Eoarchean mantle.

a: Dashed line represents a mixing line between the modern mantle composition ($\epsilon^{100}\text{Ru} = 0$) and an s-process component as defined by Ru isotope data for pre-solar silicon carbide (SiC) grains³⁴. The compositions of enstatite chondrites (EC, $\epsilon^{100}\text{Ru} = -0.08 \pm 0.04$, 95% confidence interval); ordinary chondrites (OC, $\epsilon^{100}\text{Ru} = -0.29 \pm 0.03$, 95% confidence)⁵, CI chondrites (CI, $\epsilon^{100}\text{Ru} = -0.24 \pm 0.13$, 2 s.d.)⁵; CM chondrites (CM, $\epsilon^{100}\text{Ru} = -0.69 \pm 0.38$, 95% confidence)⁵, and average carbonaceous chondrites (average CC, $\epsilon^{100}\text{Ru} = -0.90 \pm$

0.12, 95% confidence interval)⁵ are shown for comparison. The uncertainties for CI chondrites reflect a single measurement and are thus shown with the external uncertainty of the method (2 s.d. as stated in ref. 5). Uncertainties for the modern and the Eoarchean mantle composition are the same as stated in Fig. 1. Note that the uncertainty of the modern oceanic mantle composition from the literature is shown as 2 s.d.¹².

b: Plot illustrating the heliocentric zoning of $\epsilon^{100}\text{Ru}$ anomalies⁵. The presence of an s-process enriched reservoir that contributed to the Earth's growth is inferred from the Ru isotope composition obtained for the Eoarchean mantle of SW Greenland (Fig. 1). Chondrite groups formed at increasing heliocentric distances exhibit more negative $\epsilon^{100}\text{Ru}$ because they are more depleted in s-process Ru relative to Earth's modern mantle⁵. The $\epsilon^{100}\text{Ru}$ uncertainty for carbonaceous chondrites in **b** is shown as 2 s.d. to account for significant within-group variation of their $\epsilon^{100}\text{Ru}$ values (Figure modified from ref. 5).

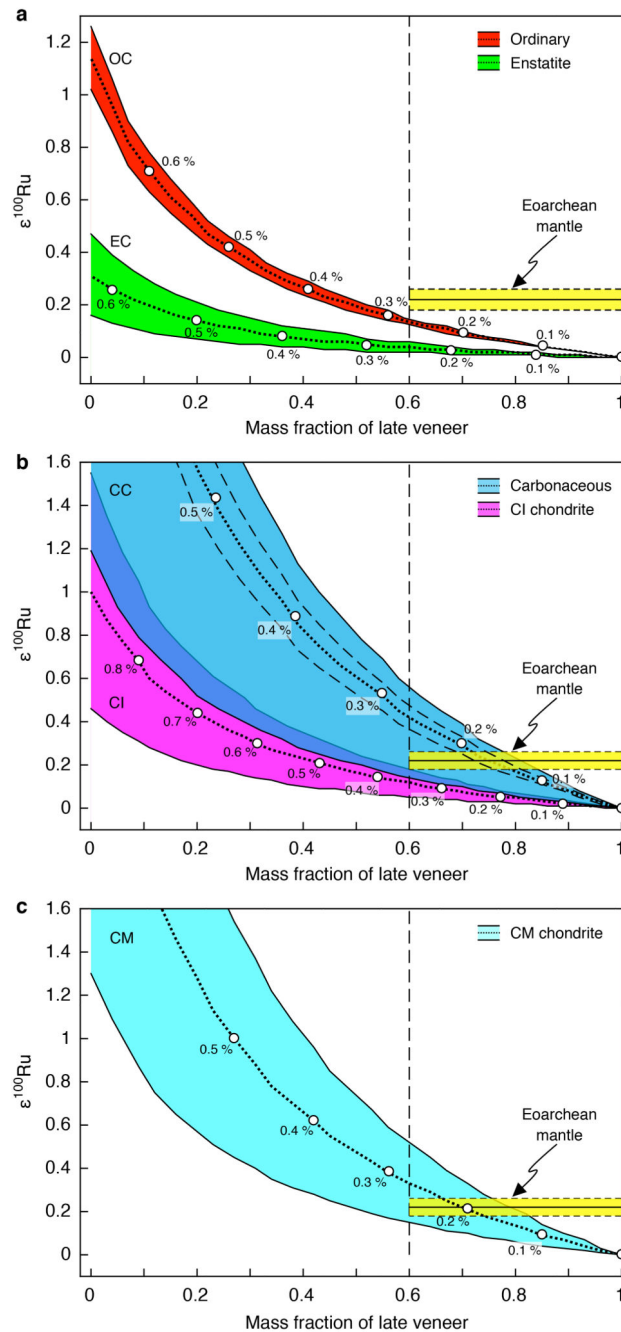


Figure 3. Model estimates for the amount of late veneer added to the Eoarchean mantle based on Ru isotope compositions.

The model illustrates the effect of subtracting variable mass fractions of late veneer from the Ru isotope composition of the modern mantle. The composition of the modern mantle was fixed at $\epsilon^{100}\text{Ru} = 0$, as indicated by the composition obtained for samples from the Bushveld complex (Extended data Table 1), which is indistinguishable from previously reported data for the modern oceanic mantle composition¹². Dotted lines indicate the respective mass fractions of different chondritic late veneer compositions subtracted from the modern mantle composition. Solid black lines show the minimum and maximum $\epsilon^{100}\text{Ru}$ values for different

chondrite classes in **a**: enstatite chondrites (EC, $\epsilon^{100}\text{Ru} = -0.08 \pm 0.04$, 95% confidence interval); ordinary chondrites (OC, $\epsilon^{100}\text{Ru} = -0.29 \pm 0.03$, 95% confidence)⁵; **b**: carbonaceous chondrites (CC, $\epsilon^{100}\text{Ru} = -0.90 \pm 0.61$, 2 s.d.; ± 0.12 , 95% confidence)⁵; CI chondrites (CI, $\epsilon^{100}\text{Ru} = -0.24 \pm 0.13$, 2 s.d.)⁵; and **c**: CM chondrites (CM, $\epsilon^{100}\text{Ru} = -0.69 \pm 0.38$, 95% confidence)⁵. The uncertainties for carbonaceous chondrites in **b** are given as 2 s.d. to account for significant within-group variation of their $\epsilon^{100}\text{Ru}$ values (dashed line indicates 95 % confidence interval uncertainty). The 2 s.d. uncertainty for CI chondrites reflects the external uncertainty of the method (as stated in ref. 5). The amount of subtracted late veneer material for each respective chondrite composition was adjusted to match a presumed Ru concentration in the pre-late veneer mantle of $\sim 1.4 \text{ ng g}^{-1}$, corresponding to $\sim 20\%$ of the Ru contained in the modern mantle. The yellow box in **a**, **b** and **c** indicates the composition of the Eoarchean mantle inferred from the mean value of all analyzed 3.8–3.7 Gyr-old samples originating from various localities of the Itsaq gneiss complex ($\epsilon^{100}\text{Ru} = +0.22 \pm 0.04$, average value shown as solid black line, dashed lines indicate 95% confidence interval uncertainty, Extended data Table 1). The solid vertical dashed line indicates the minimum late veneer contribution inferred for the mantle source of peridotite samples from the Narssaq ultramafic body (NUB) and the south of Isua supracrustal belt (SOISB), based on previously reported $^{187}\text{Os}/^{188}\text{Os}$ data and HSE concentrations¹⁴. The parameters used for the mixing model are given in Extended Data Table 3.